Dynamic transition from modelike patterns to turbulentlike patterns in a broad-area Nd:YAG laser

Eduardo Cabrera, Sonia Melle, Oscar G. Calderón, and J. M. Guerra

Departamento de Optica, Universidad Complutense de Madrid, Ciudad Universitaria s/n, 28040 Madrid, Spain

Received December 7, 2005; accepted January 9, 2006; posted January 25, 2005 (Doc. ID 66534)

We report the first experimental observation to our knowledge of a dynamic transition from modelike patterns to completely disordered patterns in a large-aspect-ratio Nd:YAG laser. Recordings of near-field patterns with an integration time as small as 1 ns allow us to follow the evolution of the transverse intensity profile along the output pulse of the laser. © 2006 Optical Society of America

OCIS codes: 190.4420, 140.3530.

Pattern formation and nonlinear dynamics have a great significance in many fields of research, including optics, hydrodynamics, and chemical reactions.[1,2] In this context the laser has become a very useful laboratory tool to study spatial self-organization phenomena that can be observed in some of these fields. In addition, the transverse structure of the laser beam determines its spatial coherence. This property can be of great importance when broad-area lasers are needed, usually in high-power applications, as can be found in laser pumping, free-space communication, or medicine.[3,4] In particular, Nd:YAG lasers have been traditionally used in these types of application thanks to their high efficiency.

There have been two main strategies to study transverse patterns in lasers. If mainly the boundary conditions impose the geometry of the field, an appropriate combination of empty cavity modes can be used to reproduce the spatial dynamics. However, if bulk parameters and nonlinearities dominate pattern formation, the system can exhibit spatiotemporal chaotic dynamics and, consequently, a very rich and complex transverse structure. The operation regime strongly depends on two parameters,[5–7] the Fresnel number and the frequency separation between transverse modes. The Fresnel number is the aspect ratio between the aperture area and the length of the cavity [$F=(b/2)^2/\lambda L$] and roughly measures the number of modes that can oscillate in the laser cavity. For our experimental setup the wavelength is $\lambda=1.06\ \mu$m, the transverse size $b=6$ mm, and the cavity length $L=17$ cm, so the Fresnel number takes the value $F\simeq 50$. Frequency separation between transverse modes, $\Delta\nu_T=c/(2\pi L)[\cos^{-1}\sqrt{1-(L/R)}]$, evaluates the strength of the interaction among these modes. Here $R=10$ m is the radius of the concave mirror. In our case $\Delta\nu_T=30$ MHz, while the width of the homogeneous line is of the order of 100 GHz. Thus, strong interaction among transverse modes takes place.

On the other hand, transverse dynamics in class B lasers has been studied mainly by looking at average patterns.[5–11] In the case of vertical-cavity surface-emitting lasers (VCSELs) the extremely fast dynamics makes it very difficult to record instantaneous snapshots of the intensity profile. Until now, only 1D streak cameras have been able to follow such a fast evolution in semiconductor lasers,[12] but no 2D time-resolved measurements have been done. In the case of CO_2 lasers, the instantaneous intensity spatial profile has been recorded along the pulse.[13] A bunch of bright peaks randomly distributed in the transverse cross section appears from the beginning of the pulse.

In Nd:YAG lasers, transverse mode dynamics was studied by Hollinger *et al.*[14] in a ring resonator. By increasing the Fresnel number of the resonator they found a transition from stable to periodic, quasiperiodic, and chaotic temporal behavior of the laser. Instantaneous transverse patterns of a *Q*-switched Nd:YAG laser were measured for a stable and for an unstable resonator configuration.[15] In Ref. 15 the Gaussian profile of the beam was selected by the system in the stable configuration along the whole evolution of the pulse, while the unstable resonator caused the growth of a ring-shaped profile. However, neither disordered patterns nor high-order modes were found in these configurations.

In this Letter we report time-resolved measurements of transverse dynamics in a pulsed custom-made Nd: YAG broad-area laser. We have seen how the pattern initially grows under the influence of boundary conditions so that modelike patterns appear. After that, nonlinearities of the medium govern the evolution, and the ordered structures are destabilized toward a highly disordered pattern, which cannot be described by cavity modes. The time needed by the system to reach this regime depends on pumping. To the best of our knowledge, this is the first observation of a dynamic transition of a laser pattern from boundary-controlled to bulk-controlled regimes. Numerical integration of Maxwell–Bloch equations has been developed, showing qualitative agreement with the experimental results.

The laser is an air-cooled, low-pulse-energy ($\simeq$50 mJ) flashlamp-pumped prototype (see Ref. 16 for a detailed description). The pumping geometry imposes an anisotropy that selects a Cartesian symmetry instead of circular symmetry. A nonpolarizing beam splitter (50:50) was placed behind the output

0146-9592/06/081067-3/$15.00

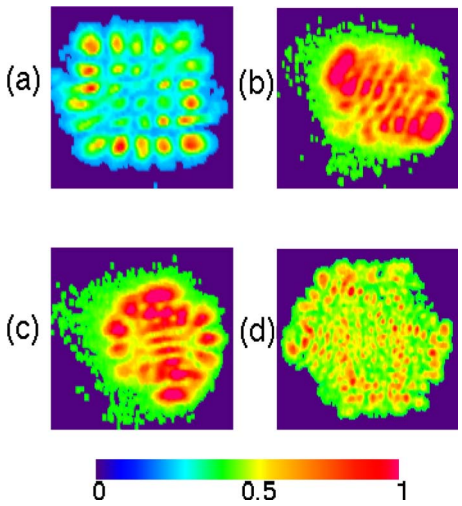

Fig. 1. (Color online) Instantaneous intensity patterns (resolution time 9 ns) for pumping 2.7 times above threshold: (a)–(c) for 4 μs of time delay from the beginning of the pulse, (d) for 40 μs of delay. Pattern size 6 mm$\times$6 mm, approximately.

coupler to separate the beams. The transmitted beam is carried to a photodiode (1 ns rise time), while the reflected beam reaches an intensified IR-enhanced CCD camera with a 768$\times$494 pixel array. The spatial resolution is 50 μm/pixel, which allows us to observe the spatial structure forming the pattern. The minimum integration time for the recorded patterns is 1 ns, much lower than the characteristic time of the local intensity evolution. We take one snapshot per pulse. Both the integration time and the time within the pulse at which we record the snapshots (time delay) are computer controlled.

Let us analyze the evolution of the pattern along the pulse for the lowest pump we can achieve (2.7 times above threshold). During the first steps of the output pulse we observe, in different pulses, two main types of ordered structure: latticelike modes and stripelike modes. Figures 1(a)–1(c) show different kinds of pattern recorded with the same time delay (4 μs). A rich variety of transverse spatial distributions can be found. In Figure 1(a) a lattice pattern that resembles a Gaussian–Hermite TEM_{45} mode can be seen. Stripelike modes with different orientations have also been observed. Figure 1(b) shows an example of this mode tilted 45°. This pattern could be characterized as a high-order Gaussian–Hermite mode or as a standing wave. To discern between the two, the instantaneous far-field patterns should be simultaneously measured with the near-field ones. More complex patterns also appear, such as the one shown in Fig. 1(c). In this case a combination of a flowerlike pattern (characterized by bright peaks around the perimeter of the laser spot) with a stripelike pattern in the vertical direction takes place. The characteristic length scale of all of these ordered structures is near 0.8 mm. The presence of this great variety of profiles for the same experimental conditions seems to indicate a weak selection of the spatial symmetry. Babushkin *et al.*[8] showed a similar coexistence of patterns for VCSEL's but for the case of stationary patterns. In that case standing waves and structures close to high-order Gaussian–Laguerre modes were seen for the same experimental conditions. Only small anisotropies selected the pattern.

The previous highly ordered patterns dramatically change along the evolution of the laser emission, leading to very disordered intensity profiles. An example of this turbulentlike behavior can be seen in Fig. 1(d), where an instantaneous pattern recorded for a time delay of 40 μs is shown. This instantaneous laser pattern consists of a bunch of bright peaks randomly distributed in the transverse cross section. In this case, we observe a mean size of the structures of 0.2 mm, much smaller than those present in the first steps of the emission. This behavior remains during the rest of the output pulse.

Increasing the pump injected into the system allows higher-order modes to overcome diffraction losses and thus to appear. This can be seen in Figs. 2(a) and 2(b), which show characteristic intensity profiles recorded for a time delay of 8 μs and a pump 4 times above threshold. Another consequence of this higher pumping is that instabilities destroy the ordered structures faster, reducing the time of the boundary-controlled regime [see Fig. 2(c)]. The lack of exact repetition of the pulses does not allow us to measure the transition time from order to disorder precisely. However, while the typical time delay to find turbulentlike patterns was 40 μs for the lowest pumping, the pattern shown in Fig. 2(c) was taken with 23 μs of delay from the beginning of the output pulse. For the highest pump we can achieve (5.4 times above threshold), no ordered patterns were observed for any time delay. The theoretical analysis has been performed by means of two-level semiclassical Maxwell–Bloch equations, with proper pumping and loss profiles. Adiabatic elimination of the electric polarization has been done to handle the system of equations numerically. In our system, time decay constants for the electric field, electric polarization, and inversion of population are, respectively $\kappa=1.4\times10^{8}\ \mathrm{s}^{-1}$, $\gamma_{\perp}=4\times10^{11}\ \mathrm{s}^{-1}$, $\gamma_{\parallel}=4.35\times10^{3}\ \mathrm{s}^{-1}$, which makes the adiabatic approximation justified. Therefore the laser equations are the following:

$$\frac{\partial E}{\partial \tau} = ia\Delta_{\perp}E + \left(\frac{D}{1+i\delta} - \eta\right)E, \qquad (1)$$

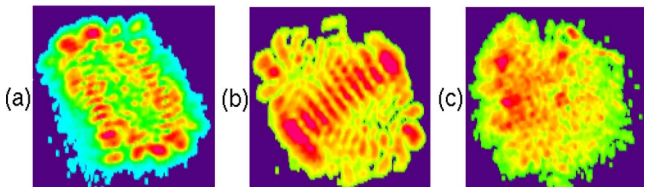

Fig. 2. (Color online) Instantaneous intensity patterns (resolution time 3 ns) for pumping 4 times above threshold (a), (b) for 8 μs of time delay from the beginning of the pulse, (c) for 23 μs of delay. Pattern size 6 mm$\times$6 mm, approximately.

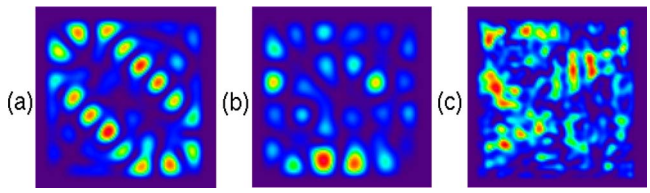

Fig. 3. (Color online) Simulated intensity patterns corresponding to different times along the laser pulse: at the beginning of the pulse (a) 3 μs, (b) 5 μs, and in the middle of the pulse (c) 50 μs. These patterns were obtained for pumping values (a) 2 times above threshold and (b), (c) 5 times above threshold.

$$\frac{\partial D}{\partial \tau} = -\gamma\left(D - R + \frac{|E|^2 D}{1+\delta^2}\right). \tag{2}$$

E and D are the dimensionless slowly varying envelopes of the electric field and of the population inversion, respectively; $\gamma \equiv \gamma_\parallel/\kappa$; $\delta = (\omega_{21} - \omega_c)/\gamma_\perp$ is the usual rescaled detuning between the atomic line center and the cavity frequency. Light diffraction is taken into account by means of the transverse Laplacian term in the field equation and is measured by the diffraction coefficient $a = c^2/(2\omega_{21}\kappa b^2)$, where b is the spatial transverse size of the laser. $\Delta_\perp = \partial_x^2 + \partial_y^2$ is the transverse Laplacian, where x and y are normalized with the spatial scale b. The time τ is normalized versus the electric field decay rate ($\tau = \kappa t$). $R(\tau, x, y)$ represents the pumping parameter. To reproduce the experimental conditions, we use a square spatial pumping profile. Likewise, the temporal form of the pumping was simulated by a function approximating the pulse excitation of the lamps. $\eta(x,y)$ takes into account the spatial dependence of the losses.

In our experimental setup there is no element introduced to select the detuning value. We can roughly estimate this value by using the well-known results of the stability analysis of the nonlasing solution for the case of a laser with infinite transverse size: $k_c = \sqrt{\delta/a}$, where k_c is the wavenumber with maximum growth at the first laser threshold. According to this expression and considering the characteristic size of the registered structures, a detuning value as small as $\delta \approx 0.01$ is obtained. So small a value will allow us to simplify the numerical calculations just by taking a zero detuning. In any case, simulations have also been developed for different detuning values close to the previous one, showing no significant changes in the spatio-temporal dynamics. Thus only the results with zero detuning are presented.

Figure 3 shows three representative instantaneous simulated patterns. In agreement with the experiment, it is found that patterns corresponding to the beginning of the pulse show highly ordered structures, whereas disordered patterns emerge for later times. Flowerlike modes and latticelike modes have been observed [see Figs. 3(a) and 3(b), respectively], although stripelike modes and more complex spatial distributions found in the experiments have not been obtained. This could be explained by the strong influence of the boundary conditions used in our simulations, which do not allow the appearance of this kind of mode. In the turbulentlike regime the patterns present smaller structures [see Fig. 3(c)], as we observed in the experiments. We have also corroborated that the lifetime of the boundary-controlled regime decreases for higher pumping. These simulations results reproduce the experimental findings with outstanding qualitative agreement.

In conclusion, we have observed for the first time a dynamic transition of laser patterns from a boundary-controlled to a turbulentlike regime. To do that, we measured instantaneous patterns with a time resolution of a few nanoseconds at various times along the pulse. Coexisting latticelike and stripelike modes appear at the beginning of the pulse. Simulations based on Maxwell–Bloch equations reproduce the main features of the experimental results.

We thank P. Hoess and J. Alonso for technical support. This work was supported by Project BFM2003-06292 (Spain). E. Cabrera's e-mail address is ecabrera@fis.ucm.es.

References

1. L. A. Lugiato, special issue on Nonlinear Optical Structure, Patterns and Chaos, Chaos, Solitons Fractals 4, 1249 (1994).
2. M. C. Cross and P. C. Hohenberg, Rev. Mod. Phys. **65**, 851 (1993).
3. M. Grabherr, M. Miller, R. Jäger, R. Michalzik, U. Martin, H. J. Unold, and K. J. Ebeling, IEEE J. Sel. Top. Quantum Electron. **5**, 495 (1999).
4. M. Miller, M. Grabherr, R. King, R. Jäger, R. Michalzik, and K. J. Ebeling, IEEE J. Sel. Top. Quantum Electron. **7**, 210 (2001).
5. G. D'Alessandro, F. Papoff, E. Louvergneaux, and P. Glorieux, Phys. Rev. E **69**, 066212 (2004).
6. D. Dangoisse, D. Hennequin, C. Lepers, E. Louvergneaux, and P. Glorieux, Phys. Rev. A **46**, 5955 (1992).
7. E. Louvergneaux, D. Hennequin, D. Dangoisse, and P. Glorieux, Phys. Rev. A **53**, 4435 (1996).
8. I. V. Babushkin, N. A. Loiko, and T. Ackemann, Phys. Rev. E **69**, 066205 (2004).
9. T. Ackemann, S. Barland, M. Cara, S. Balle, J. R. Tredicce, R. Jäger, M. Grabherr, M. Miller, and K. J. Ebeling, J. Opt. B: Quantum Semiclassical Opt. **2**, 406 (2000).
10. Y. F. Chen, K. F. Huang, H. C. Lai, and Y. P. Lan, Phys. Rev. Lett. **90**, 053904 (2003).
11. G. Huyet, M. C. Martinoni, J. R. Tredicce, and S. Rica, Phys. Rev. Lett. **75**, 4027 (1995).
12. I. Fischer, O. Hess, W. Elsäßer, and E. Göbel, Europhys. Lett. **35**, 579 (1996).
13. F. Encinas-Sanz, S. Melle, and O. G. Calderón, Phys. Rev. Lett. **93**, 213904 (2004).
14. F. Hollinger, C. Jung, and H. Weber, Opt. Commun. **75**, 84 (1990).
15. G. Anstett, M. Nittmann, A. Borsutzky, and R. Wallenstein, Appl. Phys. B **76**, 833 (2003).
16. E. Cabrera, O. G. Calderón, and J. M. Guerra, Phys. Rev. A **72**, 043824 (2005).